

On Prompt High-Energy Neutrino Emission from Gamma-Ray Bursts

Kohta Murase^{1*}

¹*Yukawa Institute for Theoretical Physics, Kyoto University,
Oiwake-cho, Kitashirakawa, Sakyo-ku, Kyoto, 606-8502, Japan*

(Dated: July 4, 2008)

Some recent observations have suggested the prompt emission at hundreds of keV from gamma-ray bursts (GRBs) could not simply be explained by the optically thin synchrotron emission. We investigate neutrino emission by using detailed numerical calculations under alternative models, the photospheric emission and synchrotron-self-Compton (SSC) emission models. In the former model, we find that neutrinos from pp reaction can be very important at energies $\lesssim (10 - 100)$ TeV. They may be detected by future neutrino telescopes such as IceCube/KM3Net and useful as a probe of cosmic-ray acceleration around/below the photosphere. In the latter model, we expect \sim EeV neutrinos produced via photomeson production. Predicted neutrino spectra are different from that in the canonical prediction, and neutrino signals would be useful as one of the clues to the nature of GRBs (the jet composition, the emission radius, the magnetic field and so on).

PACS numbers: 95.85.Ry, 98.70.Rz, 25.20.-x, 14.60.Lm

I. INTRODUCTION

High-energy neutrino emission from gamma-ray bursts (GRBs) was predicted in the standard internal-external scenario GRBs [1], and the prompt neutrino emission in the internal shock model has been studied by many authors [2, 3] (for afterglows, see Ref. [4] and references there in). However, despite the recent progresses in the *Swift* era (see reviews in, e.g., [5]), the mechanism of the prompt emission has not been well understood. One of the most frequently discussed emission mechanisms as a canonical model is the synchrotron (including diffusive synchrotron) emission, where prompt photons around the peak energy in the hard x-ray or gamma-ray band comes from electrons accelerated at internal shocks and/or by magnetic reconnection in the optically thin region. However, this model cannot satisfactorily explain some observational features such as the lower energy spectral index and observed spectral correlations [6], which may also be related to the cooling and efficiency problems [7]. Motivated by these problems, the photospheric models have been proposed [8, 9]. These photospheric models have an advantage to stabilize the peak energy identified with the thermal or Comptonized thermal peak [8, 10]. The outflow energy may internally be dissipated and thermalized at the subphotospheres, which can increase the radiative efficiency of the outflow [9, 10].

Another frequently discussed model is the synchrotron-self-Compton (SSC) emission model, which can provide viable parameter sets for the prompt emission unlike the canonical model [11]. The synchrotron peak is in the optical/ultraviolet range and gamma-ray photons arise from inverse Compton scatterings. Some bursts such as GRB 080319B may be explained [12], despite the lack of bright optical emission in many bursts [13].

In this paper, we investigate high-energy neutrino emission under these photospheric emission and SSC emission models. Our method of calculation using GEANT4 [14] is the same as in Refs. [2, 4], but quantitatively improved [15], which enables us to treat the photomeson production and pp reaction quantitatively. Various cooling processes of protons, mesons and muons are also included. As shown later, resulting spectra can be complicated, which also affects the estimate of event rates.

II. MODELS

A. Photospheric Emission Model

In the photospheric emission model, the prompt emission comes from around the photospheric radius $r \sim r_{\text{ph}}$, at which the Thomson optical depth is unity, $\tau_{\gamma e} \simeq n_e \sigma_T l$. Here, $l \approx r/\Gamma$ and Γ are the comoving width and the bulk Lorentz factor of the outflow, respectively. The baryonic photospheric radius is given by $r_{\text{ph}} \approx (L_M/4\pi\Gamma^3 m_p c^3) \simeq 1.2 \times 10^{12} \text{ cm } L_{M,52.5} \Gamma_{2.5}^{-3}$, where L_M is the kinetic luminosity of baryons. The outflows may contain copious pairs, which can extend the photospheric radius above the baryonic photospheric radius [9]. The pair photospheric radius is $r_{\text{ph}} \approx (L_{\pm}/4\pi\Gamma^3 m_e c^3) \simeq 2.2 \times 10^{14} \text{ cm } L_{\pm,51.5} \Gamma_{2.5}^{-3}$, where L_{\pm} is the kinetic luminosity of pairs. Note that smaller values of L_M or L_{\pm} lead to smaller photospheric radii, where the radiation is dominant [7]. The thermalization occurs before and/or after acceleration of the outflow, where some dissipation process around/below the photosphere may be required. In the dissipative photospheric model [9], we can assume that the dissipation is maintained after the coasting radius. Therefore, the temperature may drop as $\propto r^{-1/2}$ rather than $\propto r^{-2/3}$, which leads to the observed temperature $kT_{\text{ob}} \sim 100$ keV. Such a value is close to the observed peak energy $\varepsilon_{\text{ob}}^b$, and the Comptonized quasi-

*Electronic address: kmurase@yukawa.kyoto-u.ac.jp

thermal spectrum with $\varepsilon_{\text{ob}}^b \sim 500$ keV can be achieved by heated and/or accelerated electrons [10].

We may expect that not only electrons but also cosmic rays are accelerated around/below the photosphere, as long as the dissipation leading to particle acceleration occurs, such as internal shocks that are expected even at subphotospheres [9, 10]. The unstable pair photosphere may also lead to the dissipation and particle acceleration around the photosphere [7]. The acceleration time scale of protons is given by $t_{\text{acc}} = \eta \varepsilon_p / e B c$, and we assume the efficient acceleration with $\eta \sim 10$. The magnetic field is given by $U_B \equiv \xi_B U_\gamma$, and we hereafter assume $\xi_B = 1$. Then, the maximum energy of protons is set by the condition $t_{\text{acc}} < \min[t_p, t_{\text{dyn}}]$. Here $t_{\text{dyn}} \approx r/\Gamma c$ is the dynamical time scale and $t_p^{-1} \equiv t_{\text{BH}}^{-1} + t_{p\gamma}^{-1} + t_{pp}^{-1} + t_{\text{syn}}^{-1} + t_{\text{IC}}^{-1} + t_{\text{ad}}^{-1}$ is the proton cooling time scale, where t_{BH} , $t_{p\gamma}$, t_{pp} , t_{syn} , t_{IC} and t_{ad} are cooling time scales of the Bethe-Heitler process, photomeson production process, pp reaction, synchrotron emission, inverse Compton emission and adiabatic expansion. By using numerical calculations following Refs. [2, 4], we evaluate the maximum energy and obtain $E_p^{\text{max}} \sim 10^{8-10}$ GeV as typical values.

Sufficiently high-energy cosmic rays can interact with photons, producing mesons and muons that decay to neutrinos. The photomeson production efficiency, i.e., the effective photomeson optical depth $f_{p\gamma} \equiv t_{\text{dyn}}/t_{p\gamma}$ is estimated by using the Δ -resonance approximation [1, 2, 3, 4]. For protons at $E_p^b \sim 50$ PeV $\Gamma_{2.5}^2/\varepsilon_{\text{ob},316}^b$ keV, we obtain

$$f_{p\gamma}(E_p^b) \simeq 23 \frac{L_{\gamma,51.5}^b \Gamma_{2.5}}{L_{M,52.5} \varepsilon_{\text{ob},316}^b} \tau_{\gamma e}, \quad (1)$$

where L_γ^b is the luminosity at $\varepsilon_{\text{ob}}^b$. Hence, we can conclude that almost all the energy of high-energy protons can be used for photomeson production and accelerated protons are depleted. On the other hand, the effective optical depth for pp reaction f_{pp} is given by,

$$f_{pp} \approx \kappa_{pp} n_p \sigma_{pp} l \simeq 0.05 \tau_{\gamma e} \quad (2)$$

where $\sigma_{pp} \simeq 5 \times 10^{-26}$ cm² and $\kappa_{pp} \simeq 0.6$. Hence, we expect that a significant fraction of cosmic-ray energy is used for meson production around/below the photosphere. As seen in Eqs. (1) and (2), we obtain general relations between effective optical depths and $\tau_{\gamma e}$, which are similar to the relation between $\tau_{\gamma\gamma}$ and $\tau_{\gamma e}$ [16]. Note that we can derive similar expressions for the pair photosphere as well as the baryonic one.

For calculations of neutrino spectra shown later, we shall use the broken power-law photon spectrum for the photospheric emission from $\tau_{\gamma e} = 1$. We assume $dn/d\varepsilon \propto (\varepsilon/\varepsilon^b)^{-\alpha}$ for $\varepsilon^{\text{min}} < \varepsilon < \varepsilon^b$ or $dn/d\varepsilon \propto (\varepsilon/\varepsilon^b)^{-\beta}$ for $\varepsilon^b < \varepsilon < \varepsilon^{\text{max}}$, where we set $\varepsilon^{\text{min}} = 1$ eV, $\varepsilon^b = 1$ keV, $\varepsilon^{\text{max}} = 1$ MeV, $\alpha = 1$ and $\beta = 2.2$ [2]. On the other hand, we shall use the black-body photon spectrum for the sub-photospheric emission from $\tau_{\gamma e} > 1$, since photon spectra would be significantly thermalized. The tempera-

ture is determined by $T = (U_\gamma/a)^{1/4}$. The photon energy density U_γ is also given, assuming $U_\gamma = U_{\text{th}}$.

B. SSC Emission Model

The SSC emission model has often been discussed [11]. For example, the recently observed energetic event GRB 080319B may be explained by this model [12]. In the SSC emission model, the observed peak energy at a few hundreds of keV is identified with the second peak formed by up-scattered synchrotron photons. The first synchrotron peak is estimated as $\varepsilon_{\text{ob}}^{b1} \approx \gamma_{e,m}^2 (\Gamma e B / m_e c) \sim 10$ eV $\varepsilon_{e,-1}^2 \varepsilon_{B,-3}^{1/2} L_{M,52.5}^{1/2} r_{15.5}^{-1}$. Then, the second peak coming from inverse Compton scatterings becomes $\varepsilon_{\text{ob}}^{b2} \approx \gamma_{e,m}^2 \varepsilon_{\text{ob}}^{b1} \sim 400$ keV $\varepsilon_{e,-1}^4 \varepsilon_{B,-3}^{1/2} L_{M,52.5}^{1/2} r_{15.5}^{-1}$, which is identified with the observed peak energy $\varepsilon_{\text{ob}}^b$. Note that the third peak at ~ 10 GeV is expected, which is one of the predictions of this model. Most of the radiation energy can be released as high-energy gamma rays, so that we expect $E_\gamma^{\text{iso}} \simeq Y E_{\gamma 2}^{\text{iso}}$, where Y is the Compton Y parameter and $E_{\gamma 2}^{\text{iso}}$ is the isotropic gamma-ray energy around the second peak.

In the SSC emission model, we can also expect particle acceleration at internal shocks. Here, we shall assume the magnetic field by $\xi_B \equiv U_B/U_\gamma = 10^{-2}$, corresponding to $Y \sim 10$. Then, from the condition $t_{\text{acc}} < \min[t_p, t_{\text{dyn}}]$, we can estimate the proton maximum energy as $E_p^{\text{max}} \sim 10^{10-11}$ GeV for $\eta \sim$ a few. The maximum energy is typically limited by $t_{p\gamma}$ or t_{ad} , and production of ultra-high-energy cosmic rays (UHECRs) may be possible but not easy due to copious soft photons.

Similarly to Eq. (1), we can evaluate the effective photomeson optical depth $f_{p\gamma}$. For sufficiently high-energy protons below $E_p^{b1} \sim 500$ EeV $\Gamma_{2.5}^2/\varepsilon_{\text{ob},32}^b$ eV, we have

$$f_{p\gamma}(E_p) \simeq 3 \frac{L_{\gamma,50}^{b1}}{r_{15.5} \Gamma_{2.5}^2 \varepsilon_{32}^{b1}} (E_p/E_p^{b1})^{\beta-1}. \quad (3)$$

Hence, we expect a significant fraction of cosmic-ray energy is used for photomeson production at highest energies. But $f_{p\gamma}$ is typically rather small at lower energies, where efficient neutrino production is not expected. Note that the efficient pp reaction is not also expected due to small n_p at large radii $r \gtrsim 10^{14}$ cm.

For numerical calculations of neutrino spectra, we shall adopt the sum of multi broken power-law spectra with break energies in the comoving frame, $\varepsilon^{b1} = (10^{-2} - 10^{-1})$ eV and $\varepsilon^{b2} = 1$ keV. We also take $\varepsilon^{\text{min}} = (10^{-3} - 10^{-1})$ eV as the synchrotron self-absorption energy, and set $\alpha = 1$ and $\beta = 2.2$ as photon indices. The photon energy density $U_\gamma \equiv \int d\varepsilon \varepsilon (dn/d\varepsilon)$ is determined by $U_\gamma = E_\gamma^{\text{iso}}/(4\pi r^2 l \Gamma N)$. Here, N is the number of collisions between subshells and we take $N = 10^{1-2}$. Later, we will also calculate spectra of neutrinos, produced via photomeson interactions between protons accelerated at

the external reverse shock and prompt photons produced by internal dissipation, following Ref. [4].

III. RESULTS

We numerically calculate neutrino spectra [2, 4], although we can roughly estimate the neutrino flux from Eqs. (1)-(3). The photomeson production and pp reaction are treated in detail, taking into account the multi-pion production. We also consider various cooling processes of mesons and muons, i.e., synchrotron, inverse Compton, $\pi\gamma/\mu\gamma$, $\pi p/\mu p$ and adiabatic cooling processes. As for the cosmic-ray spectrum, we assume $dn_p/d\varepsilon_p \propto \varepsilon_p^{-2}$, expected in the first-order Fermi acceleration mechanism. The nonthermal proton energy density is expressed as $U_p = \xi_{\text{acc}} U_\gamma$, and we assume $\xi_{\text{acc}} \sim 1 - 10$ [1, 2, 3, 4].

Our numerical results of neutrino spectra in the photospheric emission model are shown in Fig. 1. Here, we assume $n_e = n_p$ for baryonic photospheric models while $n_e = (m_p/m_e)n_p$ for pair photospheric models. We can see a pp neutrino component is dominant at $E_\nu \lesssim 10$ TeV, and becomes more important as dissipation occurs at smaller radii below the photosphere. At higher energies, as the Bethe-Heitler process and photomeson production process become more important, a $p\gamma$ neutrino component is dominant. In some cases, we can see a dip feature between pp and $p\gamma$ components due to the Bethe-Heitler process (dot-dashed lines). High-energy neutrino fluxes can significantly be suppressed due to cooling of mesons and muons, since mesons and muons cool before they decay. For example, we can find break energies around PeV, and $p\gamma$ neutrinos from kaons at higher energies $E_\nu \gtrsim 10$ PeV, for Baryonic Photosphere and Baryonic Subphotosphere. Note that importance of a pp neutrino component may depend on n_e/n_p (compare thick/dot-dashed and dashed/dotted lines). In the dissipative photospheric model, we can assume that dissipation continues from subphotospheres all the way to the photosphere. In such cases, the realistic neutrino spectrum is obtained by considering contributions from various radii below the photosphere, and we expect that pp neutrinos from subphotospheres are more important at lower energies, while $p\gamma$ neutrinos from around or outside the photosphere at higher energies. If particle acceleration occurs only around the photosphere, pp neutrino fluxes are not so large (solid and dashed lines).

In Fig. 2, We show neutrino spectra in the SSC and photospheric emission models for an energetic burst such as GRB 080319B. The muon event rates expected by Ice-Cube, $N_\mu(> 10^{2.5} \text{ GeV})$, are also shown in the caption of Fig. 2. In the SSC emission model, expected neutrino signals are very few because the photon density is small at large radii. Note that neutrinos arising from protons accelerated at the reverse shock is dominant at lower energies (see SSC (RS-IS)). It is because reverse-shock protons will interact with blue-shifted prompt photons which

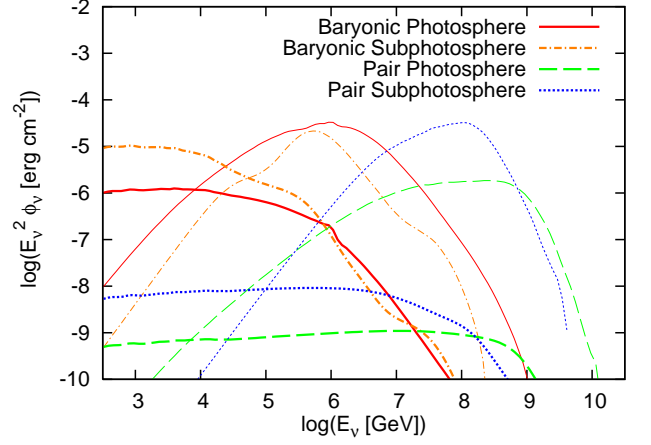


FIG. 1: The muon-neutrino ($\nu_\mu + \bar{\nu}_\mu$) fluence from one GRB event at $z = 0.1$. Thick lines show pp neutrinos while thin lines show $p\gamma$ neutrinos. Baryonic Photosphere: $r_{\text{ph}} = 10^{12.5} \text{ cm}$ ($\tau_{\gamma e} = 1$). Baryonic Subphotosphere: $r = 10^{-0.5} r_{\text{ph}}$ ($\tau_{\gamma e} = 10$). Pair Photosphere: $r_{\text{ph}} = 10^{14.2} \text{ cm}$ ($\tau_{\gamma e} = 1$). Pair Subphotosphere: $r = 10^{-0.5} r_{\text{ph}}$ ($\tau_{\gamma e} = 10$). $E_\gamma^{\text{iso}} = 10^{53} \text{ ergs}$, $\Gamma = 10^{2.5}$, $\xi_B = 1$ and $\xi_{\text{acc}} = 1$ are assumed.

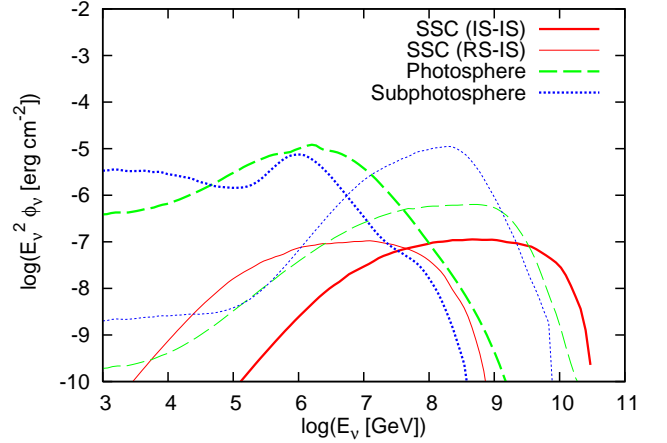


FIG. 2: As in Fig. 1, but $z = 0.9$. SSC (IS-IS) (thick solid): $r = 10^{16} \text{ cm}$, $\Gamma = 10^3$, $N = 10^2$, $\xi_B = 0.01$; $N_\mu \sim 2 \times 10^{-4}$ events. SSC (RS-IS) (thin solid): $r_\times \simeq 10^{16.4} \text{ cm}$, $\Gamma_\times \simeq 150$ and $B_\times^r \simeq 7.7 \text{ G}$; $N_\mu \sim 10^{-3}$ events. For SSC, $E_\gamma^{\text{iso}} = 10^{54.5} \text{ ergs}$, $\alpha = 0.86$, $\beta = 3.6$, $Y = 10$ and $\xi_{\text{acc}} = 1$. Photosphere (baryonic) (thick dashed): $r_{\text{ph}} = 10^{12.5} \text{ cm}$; $N_\mu \sim 0.2$ events. Photosphere (pair) (thin dashed): $r_{\text{ph}} = 10^{14.2} \text{ cm}$; $N_\mu \sim 2 \times 10^{-3}$ events. Subphotosphere (baryonic) (thick dotted): $r = 10^{-0.5} r_{\text{ph}}$; $N_\mu \sim 0.2$ events. Subphotosphere (pair) (thin dotted): $r = 10^{-0.5} r_{\text{ph}}$; $N_\mu \sim 10^{-2}$ events. For Photospheric and Subphotospheric, $E_\gamma^{\text{iso}} = 10^{54.5} \text{ ergs}$, $\xi_B = 1$ and $\xi_{\text{acc}} = 1$.

are assumed to have the steep photon spectrum $\beta = 3.6$ (solid lines) [12]. In the photospheric emission model, we may expect much larger neutrino fluences.

We may expect the time- and space-coincidence for the prompt neutrino emission. But detection of neutrinos from one burst is not easy unless the source is nearby or

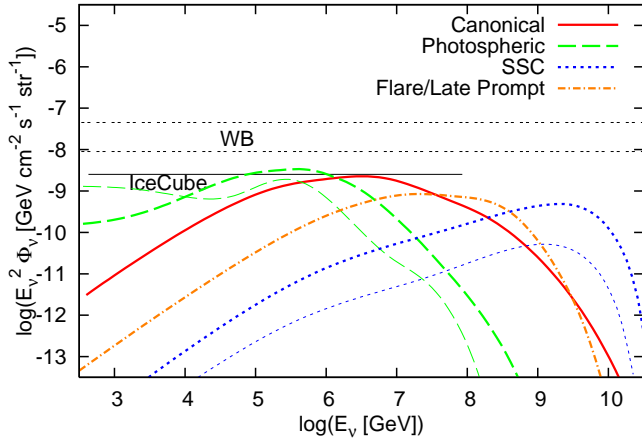


FIG. 3: The cumulative neutrino backgrounds from GRBs. Canonical: taken from Refs. [2, 4] but averaged over sets A and B, $\Gamma = 10^{2.5}$ and $\xi_B = 1$; $N_\mu \sim 9.4$ events/yr. Photospheric (baryonic) (thick dashed): $r_{ph} = 10^{12.5}$ cm, $\Gamma = 10^{2.5}$ and $\xi_B = 1$; $N_\mu \sim 24$ events/yr. Photospheric (baryonic) (thin dashed): $r = 10^{-0.5} r_{ph}$, $\Gamma = 10^{2.5}$ and $\xi_B = 1$; $N_\mu \sim 16$ events/yr. SSC (IS-IS) (thick dotted): $r = 10^{15.5}$ cm, $\Gamma = 10^{2.5}$, $N = 10$ and $\xi_B = 0.01$; $N_\mu \sim 0.14$ events/yr. SSC (RS-IS) (thin dotted): $r_\times \simeq 10^{16.9}$ cm, $\Gamma_\times \simeq 160$ and $B_\times^r \simeq 5.9$ G; $N_\mu \sim 0.014$ events/yr. Flare/Late Prompt: taken from Refs. [2, 4] (the model LP0); $N_\mu \sim 1.2$ events/yr. WB: Waxman-Bahcall bounds [1]. The cosmic-ray energy input per logarithmic interval \mathcal{E}_{HECR} is normalized to 10^{51} ergs for prompt emission models while 10^{50} ergs for Flare/Late Prompt. The GRB3 model in Ref. [4] is used with $z_{max} = 11$ under the standard Λ CDM cosmology ($\Omega_m = 0.3$, $\Omega_\Lambda = 0.7$; $H_0 = 71$ km s $^{-1}$ Mpc $^{-1}$).

energetic. Hence, it is important to consider the cumulative neutrino background. Analytically, we can estimate the background flux as [1, 2]

$$E_\nu^2 \Phi_\nu \sim 3 \times 10^{-9} \text{GeV cm}^{-2} \text{s}^{-1} \text{str}^{-1} \mathcal{E}_{HECR,51} \times \frac{f_{mes}(E_\nu)}{0.5} \frac{f_{sup}(E_\nu)}{0.5} \frac{f_z}{3} \frac{R_{GRB}(0)}{20 \text{Gpc}^{-3} \text{yr}^{-1}}, \quad (4)$$

where $f_{mes} \equiv \min[1, \max(f_{p\gamma}, f_{pp})]$, f_{sup} is the suppression factor due to cooling of mesons and muons [1, 4, 17], f_z expresses the possible contribution from high redshift sources and $R_{GRB}(0)$ is the overall local GRB rate [1, 2].

Our numerical results are shown in Fig. 3. Predicted neutrino spectra in the photospheric and SSC emission models are rather different from the canonical prediction.

In the photospheric model, we may expect larger muon event rates than other models for the same baryon loading, and pp neutrinos become important at $\lesssim (10 - 100)$ TeV energies. In the SSC emission model, we may expect $\sim (1 - 10)$ EeV neutrinos from interactions between UHECRs and soft photons, but note that our evaluation would be applied to only a fraction of GRBs [13].

IV. DISCUSSIONS

In the near future, neutrino signals may be detected by IceCube and KM3Net [18]. IceCube Deep Core for sub-TeV neutrinos, and acoustic/radio and shower detectors for \sim EeV neutrinos will also be useful. In the photospheric emission model, we can expect detectable \sim TeV neutrinos coming from pp reaction, although the spectrum and detectability can depend on the pair loading. Detection of such neutrino signals will be important as a probe of the dissipation and cosmic-ray acceleration around/below the photosphere, as well as a diagnosis of the jet composition. At higher energies, $p\gamma$ neutrinos become more important, and there may be contributions from optically thin internal shocks occurring above the photosphere. Note that neutrino signals should be correlated with the prompt gamma-ray emission, so that we can distinguish them from precursor \sim TeV neutrino signals [17]. In the SSC emission model, synchrotron photons in the optical/ultraviolet range may lead to \sim EeV neutrinos. Very high-energy neutrino signals will be useful as a probe of UHECR acceleration and may imply that emission comes from large radii, although detection of such very high-energy neutrinos is not easy. Actual GRBs might be explained by some combination of these models, where more studies in the future are needed to estimate the realistic cumulative background, considering the distribution of parameters.

Acknowledgments

As this work was being completed, we became aware, during the Nanjing GRB conference, that Wang and Dai also studied subphotospheric neutrino emission independently, albeit with a simpler formulation [19]. KM thanks X.Y. Wang for fruitful discussions there. KM also thanks P. Mészáros, K. Ioka, and S. Nagataki at the AIU 2008 conference on March, where KM gave a talk on neutrinos from around/below the photosphere. KM is supported by a Grant-in-Aid for JSPS.

-
- [1] E. Waxman and J. Bahcall, Phys. Rev. Lett. 78, 2292 (1997); E. Waxman and J. Bahcall, Phys. Rev. D 59, 023002 (1998)
 [2] K. Murase and S. Nagataki, Phys. Rev. D 73, 063002 (2006); K. Murase and S. Nagataki, Phys. Rev. Lett. 97, 051101 (2006)

- [3] C.D. Dermer and A. Atoyan, Phys. Rev. Lett. 91, 071102 (2003); D. Guetta, D.W. Hooper, J. Alvarez-Muñiz, F. Halzen, and E. Reuveni, Astropart. Phys. 20, 429 (2004); K. Asano, Astrophys. J. 623, 967 (2005); J. Becker, M. Stamatikos, F. Halzen, and W. Rhode, Astropart. Phys. 25, 118 (2006); K. Murase, K. Ioka, S. Nagataki, and T.

- Nakamura, *Astrophys. J.* 651, L5 (2006); N. Gupta and B. Zhang, *Astropart. Phys.* 27, 386 (2007)
- [4] K. Murase, *Phys. Rev. D*, 76, 123001 (2007)
- [5] P. Mészáros, *Rep. Prog. Phys.* 69, 2259 (2006); B. Zhang, *Chin. J. Astron. Astrophys.* 7, 1 (2007)
- [6] R. Preece et al., *Astrophys. J. Supplement.* 126, 19 (2000); L. Amati, *Mon. Not. R. Astron. Soc.* 372, 233 (2006)
- [7] K. Ioka et al., *Astrophys. J.* 670, L77 (2007)
- [8] P. Mészáros and M. Rees, *Astrophys. J.* 530, 292 (2000); F. Ryde, *Astrophys. J.* 625, L95 (2005); C. Thompson, P. Mészáros, and M.J. Rees, *Astrophys. J.* 666, 1012 (2007)
- [9] M.J. Rees and P. Mészáros, *Astrophys. J.* 628, 847 (2005)
- [10] A. Pe’er and Waxman, *Astrophys. J.* 613, 448 (2004) A. Pe’er, P. Meszaros, and M.J. Rees, *Astrophys. J.* 642, 995 (2006)
- [11] P. Mészáros and M.J. Rees, *Mon. Not. R. Astron.* 269, L41 (1994); A. Panaitescu and P. Mészáros, *Astrophys. J.* 544, L17 (2000); P. Kumar and E. McMahon, *Mon. Not. R. Astron.* 384, 33 (2008)
- [12] P. Kumar and A. Panaitescu, arXiv:0805.0144; J.L. Racusin et al., arXiv:0805.1557
- [13] P.W.A. Roming et al., *Astrophys. J.* 652, 1416 (2006)
- [14] S. Agostinelli et al., *Nucl. Instrum. Methods Phys. Res., Sect. A* 506, 250 (2003)
- [15] M.J. Chodorowski, A.A. Zdziarski, S.R. Sikora, *Astrophys. J.* 400, 181 (1992); S.R. Kelner, F.A. Aharonian, and V.V. Bugayov, *Phys. Rev. D* 74, 034018 (2006); K. Murase, S. Inoue, and S. Nagataki, arXiv:0805.0104
- [16] K. Murase and K. Ioka, *Astrophys. J.* 676, 1123 (2008)
- [17] P. Meszaros and E. Waxman, *Phys. Rev. Lett.* 87, 171102 (2001); S. Razzaque, P. Mészáros, and E. Waxman, *Phys. Rev. D* 68, 083001 (2003)
- [18] J. Ahrens et al., *Astropart. Phys.*, 20, 507 (2004); U.F. Katz, *Nucl. Instrum. Methods Phys. Res., Sect. A* 567, 457 (2006)
- [19] X.Y. Wang and D.G. Dai, arXiv:0807.0290